CRM

*Centre for Research in Metallurgy*
www.crm-eur.com

# *TMP'2004*

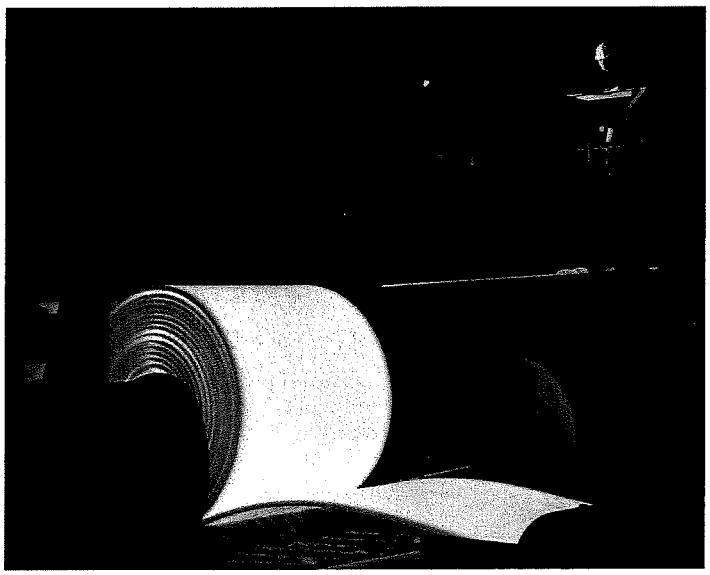

## 2nd International Conference on Thermomechanical Processing of Steels

15-17 June 2004
Liege, BELGIUM

Under the Joint Sponsorship of

The European Commission

The Province of Liege

# MESOSCOPIC MODEL OF INTERGRANULAR CRACKS IN LOW CARBON STEEL DURING COOLING OF CONTINUOUS CASTING

S. Castagne[†*], F. Pascon[†], J. Lecomte-Beckers[‡] and A.M. Habraken[†]

[†]Department M&S
[‡]Department ASMA
University of Liège, Chemin des Chevreuils 1, B-4000 Liège, Belgium

## ABSTRACT

This paper addresses the problem of transverse cracking during the continuous casting of low carbon steel. The damage mechanisms occurring at high temperature during this process are identified and a numerical approach for the modelling of these phenomena at the grain scale is proposed. Experiments allowing the identification of the model's parameters are described. Finally, the first results obtained with the model are presented.

## 1. INTROCUCTION

For low carbon steel grades, cracks generally appear in the unbending zone of the continuous casting mill. These cracks can be related to the steel grade but also to the mechanical and thermal fields occuring during the process. This paper proposes a model to investigate at the mesoscopic level the link between the integranular crack appearance and different macroscopic factors such as the shape of oscillation marks and the thermo-mechanical history during the process.

## 2. METHODOLOGY OF THE RESEARCH

The first step in the development of the mathematical model is the definition of a representative mesoscopic cell that allows the study of crack initiation and propagation at the grain level. The transfer of information between the macroscopic steel continuous casting model previously developed at the University of Liège[1] and the mesosopic cell provides the link between the mesosocpic analysis and the continuous casting process.

In order to determine the constitutive laws governing the process at the grain level, the mechanisms appearing at this level during the continuous casting of low carbon steel and leading to the apparition of cracks have first to be investigated. Having identified these mechanisms, a damage model that takes them into account can be proposed.

Microscopical, mechanical and damage experiments are performed in order to define the parameters of the model along with a literature revue.

Finally, the thermo-mechanical loadings corresponding to the continuous casting process can be applied to the mesosocpic cell. The influence of local defects, such as nozzle perturbation, roll locking or roll misalignment, on the risk of transverse crack initiation can be analysed at the grain level as well as the effect of the oscillation marks.

## 3. DAMAGE MECHANISMS IN STEEL CONTINUOUS CASTING

Brimacombe *et al.* demonstrates the importance of two zones of low ductility in steels[2]: the first one exists above 1340°C and probably accounts for the formation of all internal cracks and surface longitudinal cracks while the other lies between 700 and 900°C and is related to the appearance of transverse cracks in slabs, which is the subject of this research. To minimize crack formation, the control of the steel chemistry is absolutely essential. A lot of research work is done in this domain by metallurgists. Nevertheless, the thermo-mechanical loadings applied on the slab

[*] Currently at the Queen's University Belfast UK

during the continuous casting process also have a great influence and their analysis, as presented in this paper, is a key point in the prevention of the transverse crack initiation and propagation.

Transverse cracks in continuous casting of low carbon steels have been experimentaly shown to be intergranular[3]. They usually appear along the prior austenite grain boundaries and are characteristic of creep fracture. In the studied temperature range, cracks grow by grain boundary cavitation, due to creep plastic deformation and void diffusion, and by grain boundary sliding.

The presence of oscillation marks, which are caused by the vertical oscillations of the mould during the continuous casting, increase the susceptibility of the slab to transverse cracking. In this zone, the presence of a high segregation, whose formation mechanism has a close relation with that of oscillation marks, weaken the grain boundary[4]. Moreover, the oscillation marks behave as notches, introducing high localised stress concentrations.

## 4. NUMERICAL MODELISATION

### 4.1. Mesoscopic cell

In order to represent intergranular creep fracture, the present model contains two-dimentional (2D) finite elements for the grains and one-dimensional (1D) interface elements for their boundaries[5]. Inside the grains, an elasto-visco-plastic law without damage is used, and at its boundaries, a law with damage is preferred.

The grains are modelled by thermomechanical 4-nodes quadrilateral elements of mixed type[6]. A law of Norton-Hoff type (1) is used to quantify the visco-plastic behaviour inside the grain for the studied steel. Its expression in terms of equivalent stress, strain and strain rate is given hereafter:

$$\sigma_e = \varepsilon_e^{p_4} . exp\left(-p_1 \varepsilon_e\right) . p_2 . \sqrt{3} . \left(\sqrt{3} . \dot{\varepsilon}_e\right)^{p_3} \quad (1)$$

where the parameters $p_1$ to $p_4$ are temperature dependent.

The 2D elements modelling the grains are connected by interface elements to account for cavitation and sliding at the grain boundary. As the thickness of the grain boundary is small in comparison with the grain size, the grain boundary can be represented by 1D interface elements. These elements are associated with a constitutive law which includes parameters linked to the presence of precipitates, voids, etc. The damage variable explicitly appears in this law.

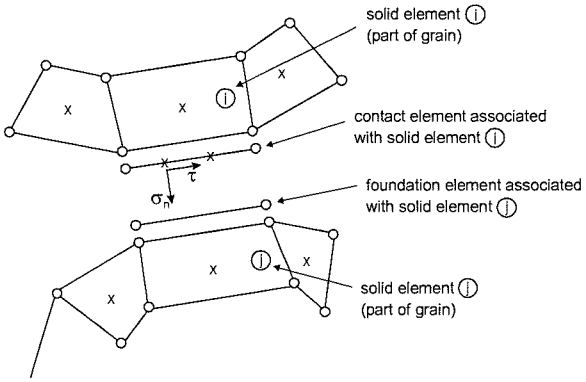


**Figure 1. Interface element: contact element, associated foundation, linked solid elements. Dots symbolize nodes and crosses represent integration points.**

The interface element is composed of a modified contact element and a foundation element (see Figure 1). For each integration point of the contact element, the program determines the associated foundation segment as well as the solid element to which the foundation is connected. The state variables for the interface element are computed using pieces of information from the two solids elements in contact (elements $i$ and $j$ in Figure 1). The state variables in the interface element are the corresponding mean values at the integration points of elements $i$ and $j$.

The original contact element was described by Habraken and Cescotto and is usually combined with a Coulomb's friction law[7]. This element has been modified in order to introduce a new interface law and a

cohesion criterion. The stress components of the interface element are represented in Figure 1, their evolution is described by the following viscoelastic-type relationships:

$$\dot{\tau} = k_s\left(\dot{u} - \dot{u}_s\right) \text{ and } \dot{\sigma}_n = k_n\left(\dot{\delta} - \dot{\delta}_c\right) \quad (2)$$

This is a penalty method where penalty coefficient $k_s$ and $k_n$ are very large to keep the deviations $\left(\dot{u} - \dot{u}_s\right)$ and $\left(\dot{\delta} - \dot{\delta}_c\right)$ small. $\dot{u}$ and $\dot{\delta}$ are respectively the relative sliding velocity of adjacent grains due to shear stress $\tau$ and the average separation rate, normal to the interface, due to damage growth. These variables are directly computed from nodal displacements. $\dot{u}_s$ and $\dot{\delta}_c$ are the same variables but related to the damage law. Their evolution are computed in the next section (Equations (3) and (14)).

### 4.2. Interface law: evolution of the damage

The relevant damage mechanisms at the mesoscale are viscous grain boundary sliding, nucleation, growth and coalescence of cavities leading to microcracks. The linking-up process subsequently leads to the formation of a macroscopic crack.

Grain boundary sliding is governed by:

$$\dot{u}_s = w\frac{\tau}{\eta_B} \quad (3)$$

where $\dot{u}_s$ is the relative velocity between two adjacent grains, $w$ is the thickness of the grain boundary and $\eta_B$ is the grain boundary viscosity. However $\eta_B/w$ can be expressed in term of the strain-rate parameter $\dot{\varepsilon}_B$ defined as follows:

$$\dot{\varepsilon}_B = \dot{\varepsilon}_0\left(\frac{w\sigma_0}{\eta_B d\dot{\varepsilon}_0}\right)^{\frac{n}{n-1}} \quad (4)$$

with $d$ a length parameter related to the grain size and $n$ the creep exponent[5]. $\sigma_0$, $\dot{\varepsilon}_0$ are reference stress and strain-rate.

In the context of damage at high temperature, the mechanism of voids nucleation, growth and coalescence is established. In most engineering alloys, cavities have been observed to continuously nucleate. The following experimental relation has been suggested:

$$\dot{N} = \beta\sigma_n^2\dot{\varepsilon}_e^C = F_n\left(\frac{\sigma_n}{\Sigma_0}\right)^2\dot{\varepsilon}_e^C \text{ with } \sigma_n \geq 0 \quad (5)$$

where $N$ is the average number of cavities per unit length of grain boundary, $\dot{\varepsilon}_e^C$ is the effective creep strain rate, $\sigma_n$ the normal stress, introduced to allow a faster nucleation on those grain boundaries which are perpendicular to the loading direction, and $\beta$ a material constant[8]. For the second formulation, $F_n$ is the nucleation parameter of the material and $\Sigma_0$ a normalization constant. $F_n$ is the microstructural parameter which influences the nucleation rate at the grain boundary. Zones where nucleation is more important can be introduced through this parameter. It can represent, among others, the precipitation state or the influence of the thin ferrite film that can form close to the grain boundary leading to strain concentration[3]. According to Equation (5), the nucleation will begin with the plastification. Nevertheless, experimentally, nucleation appears sometimes later, that is why a threshold to indicate the beginning of the nucleation has to be introduced. For this purpose, the parameter $S$ which combines the stress and the cumulated strain is defined:

$$S = \left(\sigma_n/\Sigma_0\right)^2\varepsilon_e^C \quad (6)$$

This parameter $S$ characterizes the state of the material before nucleation. It will grow with the strain and when the threshold value is reached, nucleation begins and the

parameter $S$ has no more utility. To define the threshold value $S_{thr}$, it is supposed that this threshold is related to a minimum cavity density $N_I$ from which nucleation can be observed and a factor $F_n$ indicating the importance of the nucleation activity of the material:

$$S_{thr} = N_I / F_n \tag{7}$$

Finally, experience shows that the cavity density tends to saturate for large creep strains, then the nucleation of new cavities stops when $N$ reaches the value $N_{max}$. If $2b$ is the cavity spacing, $N$ is related to it by $N = 1/\pi b^2$. We have:

$$\dot{b} = -\frac{1}{2}\frac{\dot{N}}{N} b = -\frac{\pi}{2} b^3 \beta \sigma_n^2 \dot{\varepsilon}_e^C \tag{8}$$

The nucleation rate $\dot{N}$ is related to the internal state of the material $N$ as well as to the stress $\sigma_n$ and strain rate $\dot{\varepsilon}_e^C$ states on the grain boundary. With a one-dimensional element, this nucleation rate $\dot{N}$ can be interpreted as a measure of the rate of evolution of the cavity spacing $\dot{b}$. This equation can be used to compute the decrease rate of $b$ due to continuous nucleation of cavities.

A detailed formulation of the cavity growth under diffusion and creep deformations was proposed by Tvergaard[9]. An idealized formulation of the grain boundary geometry is used: the cavities are supposed to be uniformly distributed with an average spacing of $2b$ and a diameter of $2a$ as represented in Figure 2.

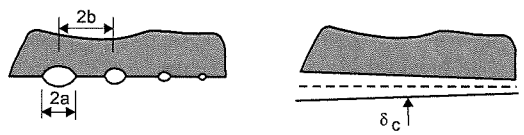


**Figure 2. Discrete and continuous representations of the grain boundary.**

For the proposed idealized boundary geometry with a cavity tip angle $\Psi$, the cavity growth rate is:

$$\begin{aligned} \dot{a} &= \dot{V} / \left[ 4\pi a^2 h(\Psi) \right] \\ &= \left( \dot{V}_1 + \dot{V}_2 \right) / \left[ 4\pi a^2 h(\Psi) \right] \end{aligned} \tag{9}$$

where $h(\Psi) = \dfrac{(1+\cos\Psi)^{-1} - 0.5\cos\Psi}{\sin\Psi}$

(shape function of the cavity) and $\dot{V}$ is the total cavity volume growth rate, which is divided into diffusion growth $\dot{V}_1$ and creep deformation $\dot{V}_2$:

$$\dot{V}_1 = 4\pi D \frac{\sigma_n}{\ln(1/f) - (3-f)(1-f)/2} \tag{10}$$

$$\dot{V}_2 = \begin{cases} -A\left( \dfrac{3}{2n}\left|\dfrac{\sigma_m}{\sigma_e}\right| + N \right)^n & \text{for } \dfrac{\sigma_m}{\sigma_e} < -1 \\ A\left( \dfrac{3}{2n} + N \right)^n & \text{for } \left|\dfrac{\sigma_m}{\sigma_e}\right| \le 1 \\ A\left( \dfrac{3}{2n}\dfrac{\sigma_m}{\sigma_e} + N \right)^n & \text{for } \dfrac{\sigma_m}{\sigma_e} > 1 \end{cases} \tag{11}$$

where $N = \left[ (n-1)(n+0.4319) \right] / n^2$ and $A = 2\pi \dot{\varepsilon}_e^C a^3 h(\psi)$. $D$ is a constant related to the material diffusion, $n$ the creep exponent, $\sigma_n$, $\sigma_e$ and $\sigma_m$ are respectively the normal, effective, and mean stresses applied on the grain boundary. The variable $f$ is defined as follows:

$$f = max\left\{ (a/b)^2, \left[ a/(a+1.5L) \right]^2 \right\} \tag{12}$$

where $L = \left( D\sigma_e / \dot{\varepsilon}_e^C \right)^{1/3}$.

The coupling between diffusive and creep contribution to void growth is introduced trough the length scale $L$: for small values of $a/L$, cavity growth is dominated by diffusion while for larger values, creep growth becomes more and more important.

The diffusion parameter can be expressed as a function of the temperature by:

$$D = \frac{D_{b0}\delta_b \Omega}{kT} \cdot exp\left(-\frac{Q_b}{RT}\right) \qquad (13)$$

with $D_{b0}\delta_b$ the grain boundary diffusion coefficient, $\Omega$ the atomic volume, $Q_b$ the activation energy, $T$ the temperature in Kelvin, $k$ the Boltzmann's constant and $R$ the molar gas constant. The particular values for austenitic steel are the following[10]: $D_{b0}\delta_b = 7.5\ 10^{-14}$ m$^5$/s, $\Omega = 1.21\ 10^{-29}$ m$^3$ and $Q_b = 159$ kJ/mol.

Finally the discrete cavity distribution is replaced by a continuous distribution on each facet of the grain boundary so that the cavity volume $V$ and the average separation between two grains $\delta_c$ evolve in a continuous way on the facet (see Figure 2). Then, the separation rate is given by:

$$\dot{\delta}_c = \frac{\dot{V}}{\pi b^2} - \frac{2V}{\pi b^2}\frac{\dot{b}}{b} \qquad (14)$$

Coalescence takes place when cavities are sufficiently close to each other to collapse. At this moment, the crack begins to propagate and the interface elements are no more in contact. The parameter used to define the coalescence activation is the ratio $a/b$. We call it a damage variable in the current model. When this ratio reaches a critical threshold, coalescence is triggered and crack appears.

### 4.3. Meso-macro link

In this research, the continuous casting process and the damage evolution is analysed at the grain scale and specific study zones have to be defined for the finite element calculations. Indeed, it is not conceivable to model the whole slab at the mesoscopic scale.

The macroscopic continuous casting model available in the University of Liège[1] provides various results such as temperature field, thickness of the solidified shell, stress, strain and strain rate fields in the strand which will be used in combination with the mesoscopic model. It also computes some crack risk indicators in agreement with industrial observations showing that transverse cracks always appear near the edge of the slab and at its surface and indicating that the mesocopic cell has to be chosen in this zone.

To allow the transfer of data from the macroscopic model, the mesoscopic cell is surrounded by a transition zone. The history of forces and/or displacements known thanks to the macroscopic simulation is imposed on each node of the boundary of the transition zone. It is important to follow the whole process as we use elasto-visco-plastic constitutive laws.

At each time step, the temperature of each node of the mesoscopic cell is fixed according to the results of the macroscopic simulation and no thermal exchange is computed at this scale. The whole thermal problem has already been treated by the macroscopic model.

Results of simulations are presented in section 6 after the description of the experimental analysis realised to identify the parameters of the model.

## 5. EXPERIMENTAL PROGRAM

The material was provided in the form of blocks cut in a reject slab. Three categories of experiments have been performed in order to define the parameters to be introduced in the model: metallographic, mechanical and damage analysis.

### 5.1. Metallographic analysis

Metallographic analysis combining optical microscopy and picric acid etching on steel samples, have been performed at room temperature to determine the original austenitic grain size and morphology. Figure 3 shows an example of the austenitic microstructure.

The grain size was measured using the planimetric method describe in the ASTM E112 standard[11]. This method consists in

counting the number of grains contained in a 5000 $mm^2$ circle. Knowing the scale of the picture it is then possible to transform this number of grains into an equivalent grain diameter. It was found that on a facet parallel to the lateral fac e of the slab, close to this lateral face, the grain size evolves from 1 mm at the corner of the slab to 1.5 mm in the middle. As the cracks usually appears close to the corner of the slab, an average austenitic grain size $d$ of 1 mm has been introduced in Equation (4), which is actually a huge grain size.

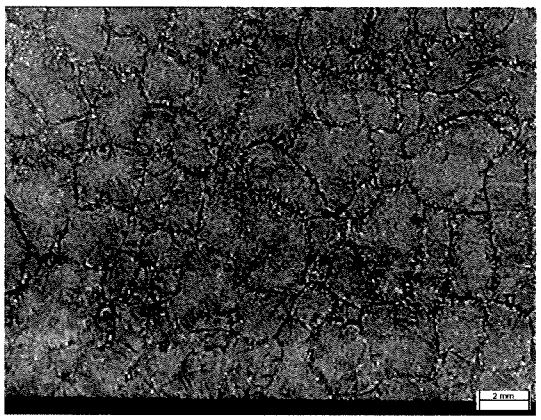


**Figure 3. Austenitic microstructure of the studied steel at mid-height of the slab close to the lateral face on a facet parallel to this lateral face.**

The microscopic images have also been used to define a representative finite element mesh of the grains microstructure in the mesosocpic cell.

Figure 4 represents one of the meshes used for the numerical simulations performed to identify the damage parameters (see section 5.3).

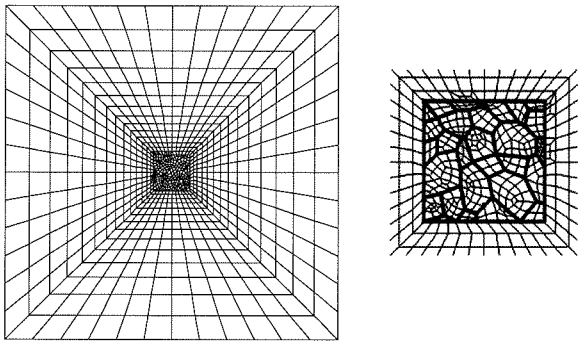

**Figure 4. Left: mesoscopic cell surrounded by a transition zone (50 mm x 50 mm). Right: zoom on the grains zone (5 mm x 5 mm).**

## 5.2. Mechanical analysis

Compression tests of cylindrical samples have been performed and the corresponding stress-strain curves recorded. Various strain rates (0.01, 0.001, 0.0001 $s^{-1}$) and temperatures (700, 800, 900, 1000 and 1100 °C) have been tested in order to identify the parameters $p_1$ to $p_4$ of Equation (1). A thermal treatment that aimed at reproducing the thermal cycle of continuous casting had been applied on each test sample before compression.

The results of the identification can be found in Table 1. $p_1$ represents the effect of softening, $p_2$ is linked to the level of the curve, $p_3$ models the viscosity and $p_4$ the hardening. $p_1$ does not influence the results of the macroscopic continuous casting model as it has principally an effect in the large strains that will not appear in this process. Nevertheless, it is important to have an accurate model at larger strains for the acoustic tests simulations and in case of localised higher strains due to the grain configuration in the mesoscopic cell. $p_3$ and $p_4$ lie almost in the interval 0.1 – 0.2, which fits with the classical values used for steel. $p_3$ does not increase monotonously as could have been expected for the majority of steel grades. Nevertheless, this type of behaviour can be found in literature for several low carbon steel grades[12], which is precisely the type of steel we are studying here.

**Table 1. Parameters of the Norton-Hoff law.**

| $T$ [°C] | $P_1$ | $P_2$ | $p_3$ | $p_4$ |
|---|---|---|---|---|
| 700 | 0.2476 | 156.107 | 0.115 | 0.067 |
| 800 | 0.7749 | 303.085 | 0.231 | 0.203 |
| 900 | 0.0465 | 125.001 | 0.155 | 0.210 |
| 1000 | 0.0014 | 53.692 | 0.099 | 0.193 |
| 1100 | 0.8429 | 65.402 | 0.148 | 0.193 |

## 5.3. Damage analysis

The damage analysis consists in acoustic tests realised on steel samples in order to determine the apparition of the first crack during compression. At the origin, the tests were developed at the IBF in Aachen to predict the formality of the steel at low temperature and were then adapted to the

condition prevalent during hot forming[13]. The same concept as for the forming limit diagrams is used but here for massive samples and not for sheets.

The goal of these tests is to provide a set of experiments to identify the parameters of the interface law. Sets of acoustic tests have been done with different sample geometry (two cylindrical and one concave) to realize different stress-state histories at the critical point of a sample where the crack is supposed to appear due to mechanical loading. After having been thermally treated to reproduce the thermal cycle of continuous casting, the samples have been compressed up to crack initiation with a constant strain rate while upcoming acoustic emission events caused by material failure have been recorded. Three temperature (800°C, 900°C, 1000°C) and two strain rates (0.001 $s^{-1}$, 0.0005 $s^{-1}$) have been tested with at least three samples for each combination and for each geometry to ensure a statistically relevant result.

The finite element simulations of these tests give the formability curve and also the strain and temperature state in all samples and in particular in the region around the crack. These data are used in combination with the cellular model (Figure 4) to identify and validate the parameter of the interface law. The methodology for the transfer of data between the macroscopic compression simulation and the mesoscopic cell is the same as explained in section 4.3. This work is still in progress.

## 6. NUMERICAL RESULTS

Initiation and growth of cracks for the simple loading of Figure 5 is simulated as a first application. For this example, the parameters of the interface law are issued from literature[5] as their identification according to the damage experiments has not been completed yet. The displacement rate is chosen to obtain strain rates compatible with those usually encountered in continuous casting. The mesh is defined on the basis of the micrographs of section 5. The size of the mesoscopic cell is 5 mm x 5 mm and it is surrounded by a transition zone (10 mm x 15 mm). The right border of the grain zone is left free to allow the crack to propagate.

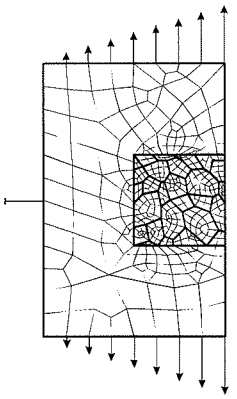

**Figure 5. Imposed displacements.**

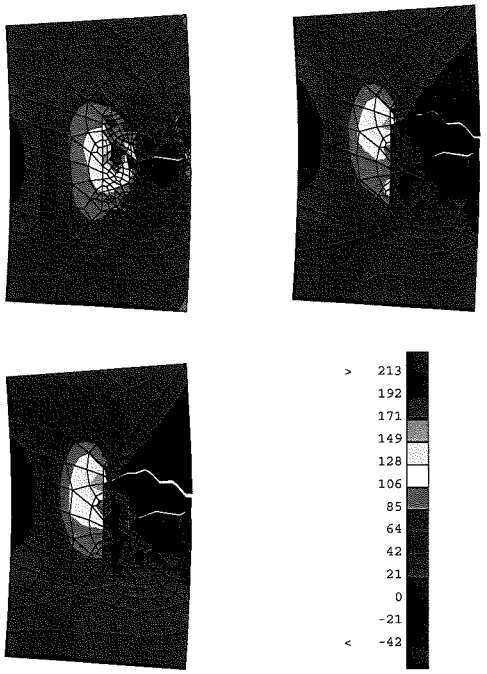


**Figure 6. Stress maps: $\sigma_m$ [Mpa] at different steps of the crack propagation.**

The initiation and propagation of two cracks can be seen in Figure 6. The mean stress increases at the crack tip while decreasing on the lips the crack. In this example, the crack goes deep into the material and a bigger cell could be used to avoid the perturbations at the junction between the transition zone and the grain zone. Indeed, cracks can not propagate into

the transition zone where no interface elements are present.

This first example shows the ability of the finite element code to model a crack which is propagating.

## 7. CONCLUSIONS AND FUTURE WORK

A model for crack initiation and propagation in steel at high temperature is available and the experiments to determine its parameters have been realised. The identification of the parameters of the interface law is in progress comparing the results of the damage experiments with finite element simulations.

Thanks to the macroscopic continuous casting model[1], the critical zones to take into account and the loadings to apply to the mesoscopic cell are known. The next step is the application of these loadings to the grain cell and the study of the influence parameters such as grain size or the oscillation marks as well as the analysis of particular defects occurring in the continuous casting machine.


## ACKOWLEDGEMENTS

As Research Associate of the National Fund for Scientific Research, A.M. Habraken thanks this Belgian research fund for its support. The industrial partner ARCELOR, its research team IRSID and the Technical Direction of Cockerill Sambre are acknowledged as well as IBF where part of the experimental study was realised.


## REFERENCES


1. F. Pascon and A.M. Habraken, "2D½ Thermo-Mechanical Model of Continuous Steel Casting Using F.E.M.", *6th Esaform Conference on Metal Forming,* Salerno, Italy, edited by V. Brucato at Nuova Ipsa Editore, 2003, 759-762.
2. J.K. Brimacombe and K. Sorimachi, "Crack Formation in the Continuous Casting of Steels", *Metallurgical Transactions B*, 8, 1977, 489-505.
3. B. Mintz, S. Yue and J.J. Jonas, Hot Ductility of Steels and its Relationship to the Problem of Transverse Cracking during Continuous Casting, *International Material Reviews*, 36, 1991, 187-217.
4. S. Harada, S. Takana, H. Misumi, S. Mizogichi and H. Horiguchi, "A Formation Mechanism of Tranverse Cracks on CC Slabs Surface", *ISIJ International*, 30, 1990, 310-316.
5. P. Onck and E. van der Giessen, "Growth of an Initially Sharp Crack by Grain Boundary Cavitation", *J. Mech. Phys. Solids*, 47, 1999, 99-139.
6. Y. Zhu and S. Cescotto, "Unified and Mixed Formulation of the 4-Node Quadrilateral Elements by Assumed Strain Method: Application to Thermomechanical Problems", *Int. J. Num. Meth. Eng.*, 38, 1995, 685-716.
7. A.M. Habraken and S. Cescotto, "Contact between Deformable Solids: the Fully Coupled Approach", *Mathl. Comput. Modelling*, 28, 1998, 153-169.
8. E. van der Giessen and V. Tvergaard, "Development of Final Creep Failure in Polycrystalline Aggregates", *Acta Metall.*, 42, 1998, 959-973.
9. V. Tvergaard, "On the Creep Constrained Diffusive Cavitation of Grain Boundary Facets", *J. Mech. Phys. Solids*, 32, 1984, 373-393.
10. A. Needleman and J.R. Rice, "Plastic Creep Flow Effects in the Diffusive Cavitation of Grain Boundaries", *Acta Metallurgica*, 28, 1980, 1315-1332.
11. American Society for Testing and Materials, "Standard Method for Determining Average Grain Size", *ASTM E112*, 1996.
12. T. Altan, S. Oh and H. Gegel, *Metal Forming Fundamentals and Applications*, published by ASM, 1983, 60-61.
13. R. Kopp and G. Bernrath, "The Determination of Formability for Cold and Hot Forming Conditions", *Steel Research*, 70, 1999, 147-153.